Prolonged and Extremely Non-radial Solar Wind Flows

Susanta Kumar Bisoi[1,*], Diptiranjan Rout[2], Janardhan Padmanabhan[3], Ken'ichi Fujiki[4], Dibyendu Chakrabarty[5] and Karan Sahu[1]

[1] Department of Physics and Astronomy, National Institute of Technology, Rourkela–769008, India

[2] National Atmospheric Research Laboratory, Gadanki, India

[3] Astronomy & Astrophysics Division, Physical Research Laboratory, Navrangpura, Ahmedabad, India

[4] Institute for Space-Earth Environmental Research, Nagoya, Japan

[5] Space & Atmospheric Science Division, Physical Research Laboratory, Navrangpura, Ahmedabad, India

* Corresponding author: bisois@nitrkl.ac.in

Abstract

We present a study of three highly non-radial solar wind events in which the azimuthal solar wind flow angle exceeds 6° for one day or more. None of the events are associated with coronal mass ejections and co-rotating interaction regions observed at 1 AU. For all events, the solar wind outflows at 1 AU exhibit low velocity and density. Based on the significant increase in the oxygen charge-state ratio of O^{7+}/O^{6+} at 1 AU for all of the events, we have traced them back to the Sun and found that their source regions originated in active region and coronal hole (AR–CH) pairs mainly located at the central meridian. Furthermore, examining the dynamical evolutions in their source regions using both the Extreme ultra-violet Imaging Telescope and the Michelson Doppler Imager, we found that the changes taking place in AR–CH boundaries eventually disturbed the stable CH configurations, resulting in a reduction of the CH area and finally its disappearance, leaving only with the AR. Our study provides a possible explanation for discussing the origin of the prolonged and highly non-radial solar wind flows.

Keywords: Solar Wind, Non-radial Solar Wind, Space Weather

1. Introduction

The high temperature of the solar corona (10^6 K) facilitates the escape of coronal plasma from the Sun's gravitational potential well, allowing it to flow upward along open magnetic field lines to form the solar wind. The solar wind carries the frozen-in magnetic field out to 1 AU and beyond in the well-known *Parker spiral* pattern, resulting in generally radial flow beyond the Alfvén radius (R_A). However, there have occasionally been observations of highly

non-radial solar wind flows, where the azimuthal component of the solar wind velocity (V_y) was going well above the usual range of 10 to 30 km/s or the azimuthal solar wind flow angle ($\Phi_v = \arctan(-V_y/V_x)$) was greater than $6°$. V_x and V_y are, respectively, the x- and y-components of the solar wind velocity, defined in the geocentric solar ecliptic (GSE) coordinate system. In this system, the x-axis points toward the Sun, the y-axis lies in the ecliptic plane and points towards the dusk, and the z-axis is parallel to the ecliptic pole along the positive north direction. Primarily, high non-radial flows have been observed when the solar wind flows were associated with coronal mass ejections (CMEs) or their interplanetary counterparts, i.e., interplanetary coronal mass ejections (ICMEs), where the azimuthal component of solar wind velocity can be significantly higher (≥ 100 km/s, Owens and Cargill, 2004). Generally, CMEs/ICMEs are fast-moving and contain a well-defined magnetic cloud. The magnetic field structures within the ICME and its embedded magnetic cloud are observed to be anchored to the Sun's surface even when they arrive at 1 AU. The highly non-radial flows due to CMEs occur because of the deflection of the solar wind plasma around the draped magnetic field structures. The draping of the magnetic field structures occurs around the CME plasmoid because of the low beta plasma condition, which arises due to the expansion of the CME cloud in space. Besides CMEs, highly non-radial flows have also been observed for co-rotating solar wind structures, such as co-rotating interaction regions (CIRs; Gosling and Pizzo, 1999). A stream interaction region (SIR) usually forms when the faster solar wind originating from the coronal holes (CH) overtakes the background slower solar wind (Jian et al., 2006; Richardson, 2018). They are classified as CIRs when they exist for at least one complete solar rotation (Jian et al., 2006). The compression of the faster and slower solar wind streams makes the solar wind flow non-radial for a few hours during the passage of CIRs.

Highly non-radial flows, lasting over 24 hours, have also been observed in the absence of CMEs/CIRs, and are known as "solar wind disappearance events" (Janardhan et al., 2008a,b). During these events, other than highly non-radial flows, low density ($< 0.1\,\mathrm{cm}^{-3}$), low velocity ($< 350\,\mathrm{km\,s}^{-1}$) solar wind outflows associated with large flux expansion factors, and extended Alfvén radii are observed (Janardhan et al., 2005). The solar sources of these unique events are found to be small, short-lived (24–48 hours), transient mid-latitude CH (Kahler and Hudson, 2001), located at the central meridian and adjacent to active regions (AR). For such a solar wind disappearance event on 11 May 1999, Janardhan et al. (2008b) suggested that the dynamical evolution of the AR and CH pinch-off the transient solar wind outflow coming from the CH to result in a low solar wind density at 1 AU. In the present study, a detailed investigation has been carried out on three extreme non-radial events where the solar wind flow angle exceeded $6°$ for 24 hours or more, and no CMEs/CIRs were observed during any of the events.

2. Observations

2.1. The events of 10–12 May 1999, 27–30 March 2000 and 15–18 February 2004

Figure 1 presents observations of solar wind plasma and magnetic field parameters in the GSE coordinate system at the first Lagrangian point (L1) from the OMNI database, plotted as a function of the day during the events of May 1999 (left), March 2000 (middle) and February
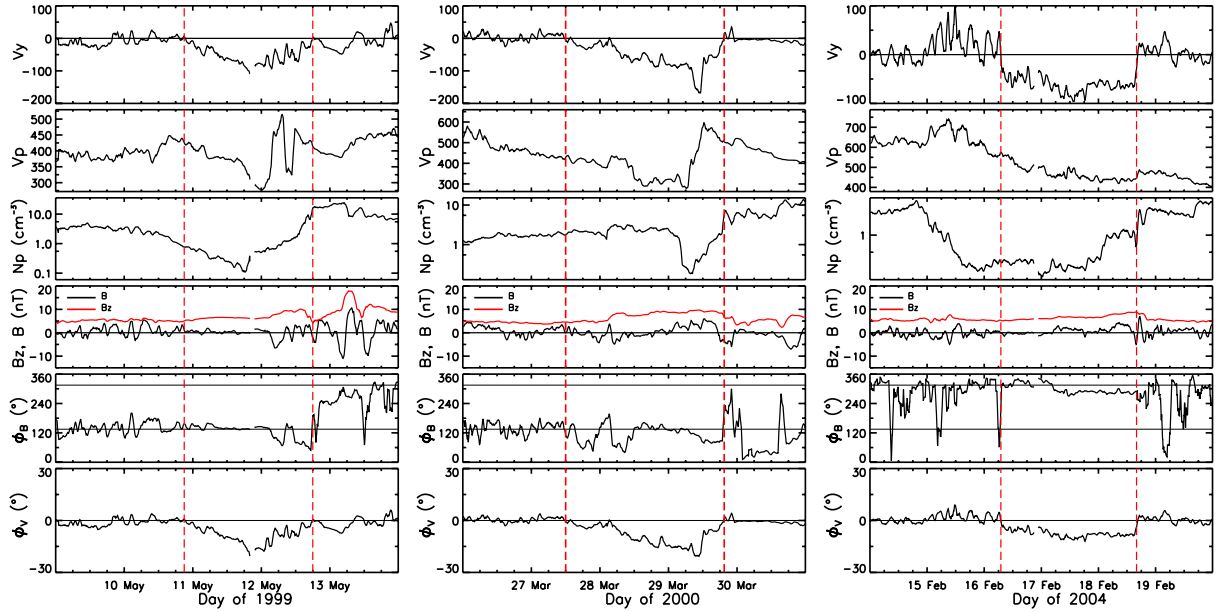
Figure 1: Variations for solar wind parameters for the events of May 1999 (*left*), March 2000 (*middle*), and February 2004 (*right*). The parameters (from *top* to *bottom*, are the *y*-component of the solar wind velocity (V_y), the solar wind flow velocity (V_p), the proton density (N_p), the *z*-component of the interplanetary magnetic field (B_z), the magnetic field strength ($|B|$), the solar wind azimuthal magnetic field angle (Φ_B), and the solar wind azimuthal flow angle (Φ_v), respectively. The red vertical lines demarcate the duration of non-radial solar wind flows.

2004 (right). In each panel, the solar wind plasma and magnetic field parameters, from top to bottom, are the *y*-component of the solar wind velocity (V_y), the solar wind flow velocity (V_p), proton density (N_p), the *z*-component of interplanetary magnetic field (B_z), the magnetic field strength ($|B|$), the solar wind azimuthal magnetic field angle (Φ_B), and the solar wind azimuthal flow angle (Φ_v), respectively. As mentioned before, the large values of both V_y and Φ_v indicate the non-radial flow nature of the solar wind. It is evident from Fig. 1 (left) that Φ_v has been non-radial since about 21:00 UT on 10 May 1999, and after that, it remained non-radial for the next 44 hours. The non-radial flow of the solar wind is also evident from the negative value of V_y, reaching as high an absolute value as $\sim 125\,\mathrm{km\,s^{-1}}$. The strength of the V_p also continuously decreased. Similarly, a continuous reduction in N_p has been observed, remaining $< 1\,\mathrm{cm^{-3}}$ for more than 24 hours. On the other hand, B_z was mostly northward, and its magnitude always hovered around the zero line, while the value of $|B|$ remained steady.

Φ_v is also negative since 13:00 UT on 27 March 2000, as evident from Fig. 1 (middle), and remained negative for the next 56 hours. Further, continuous negative variations of V_y confirm the non-radial flow of solar wind during the March 2000 event. During the non-radial flow of solar wind, V_p values were reduced. The value of N_p also remained below $1\,\mathrm{cm^{-3}}$ for a continuous ~ 18 hours. On the other hand, B_z was mostly northward, and $|B|$ nearly steady during the non-radial flow interval. Figure 1 (right) shows another long-duration non-radial flow
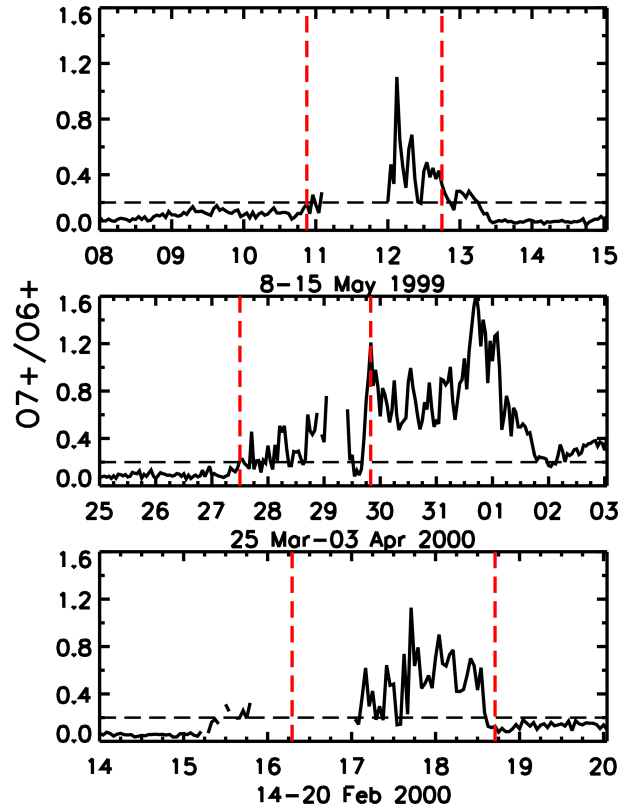
Figure 2: O^{7+}/O^{6+} charge-state ratio for the periods of 8–15 May 1999 (*top*), 25 March–3 April 2000 (*middle*), and 14–20 February 2004 (*bottom*). A horizontal dashed line is drawn at an O^{7+}/O^{6+} ratio of 0.2, while the vertical dashed lines in red demarcate the period corresponding to the non-radial flow, as indicated in Fig. 1. During this eriod, the oxygen charge-state ratio is well above 0.2.

event in February 2004. It is evident from Fig. 1 (right) that the solar wind flow is non-radial for around 58 hours, showing a negative value for Φ_v during the period from 15 to 18 February 2004. A continuous negative value of V_y is seen during the period, further showing the solar wind's prolonged non-radial flow nature during 15–18 February 2004. In addition, the solar wind velocity shows continuous reductions. However, it never fell below $400\,\mathrm{km\,s}^{-1}$, and B_z mostly hovers around the zero line, as during the earlier events. The non-radial solar wind flow also has a low density, less than $1\,\mathrm{cm}^{-3}$ for over two days.

The oxygen charge-state ratio (O^{7+}/O^{6+}), measured at L1 by the Advanced Composition Explorer (ACE) satellite, is plotted in Fig. 2 for the events of May 1999 (top), March 2000 (middle), and February 2004 (bottom).

The solar wind from AR sources usually has a higher O^{7+}/O^{6+} ratio (0.1–0.6) than that from CH regions (0.2, Liewer et al., 2004). It is evident from Fig. 2 that the oxygen charge-state ratio O^{7+}/O^{6+} was below 0.2 and started to increase for all the events at the time when the solar wind flow became highly non-radial. It is to be noted that the oxygen charge-state ratio was well above 0.2 for the whole duration of non-radial flow, as demarcated by the vertical lines in red in each panel of Fig. 2. The O^{7+}/O^{6+} ratio greater than 0.2 indicates a clear transition of

1007

solar wind source regions from CH to AR.

2.2. Source region locations

It is evident from Fig. 2 that the source regions of the prolonged and highly non-radial solar wind flows showed a clear transition from a CH to an AR located near the CH during the non-radial flow event period. Thus, in the first step, a velocity traceback method has been employed to find the source regions of the non-radial flow events. In the traceback method, the solar wind flows during the event period are tracked back using in-situ measurements of solar wind speed from the ACE spacecraft at L1 to the source surface at $2.5 R_\odot$. The event period at the source surface corresponding to the event at 1 AU is the traceback date. The velocity traceback technique is usually employed for steady-state solar wind flows. However, it has also been successfully used even for the highly non-radial flow events (e.g., Balasubramanian et al. (2003), Janardhan et al. (2005), Janardhan et al. (2008a) and Janardhan et al., 2008b) during the well-known solar wind disappearance event of 11 May 1999. In the second step, extrapolated magnetic fields are computed up to the source surface by applying a potential field model (Hakamada and Kojima, 1999) to a photospheric synoptic magnetic map. The computed field lines are then used to trace the footpoints of the field lines from the source surface to the photosphere.

Subsequently, the background magnetic field conditions on the Sun during our period of interest are investigated.

Synoptic maps showing the heliographic latitudes and longitudes of strong magnetic fields during Carrington rotations (CR) 1949, 1961, and 2013 are depicted in Fig. 3 (top), (middle) and (bottom), respectively, corresponding to the events of May 1999, March 2000 and February 2004. These synoptic maps were generated using magnetograms obtained from the Michelson–Doppler-Imager (MDI; Scherrer et al., 1995) instrument on board the Solar and Heliospheric Observatory (SOHO; Domingo et al., 1995) spacecraft. In each synoptic map, the dates of the central meridian passage (CMP) are marked at the top, while the heliographic longitude ranging from 0° to 360° (indicated by two dotted vertical lines) and latitude from −90° to 90° are marked on the abscissa and the ordinate, respectively. In Fig.3, the potential field computed source surface magnetic fields lie in an equally spaced grid along the equator. On the other hand, their radially back-projected photospheric footpoints are clustered in tightly bunched regions associated with active regions north and south of the equator. The footpoints mark the source regions of the open magnetic field lines that connect from 1 AU to the Sun at the time of the event. The groups of converging red and magenta lines shown in Fig. 3 depict magnetic field lines that join the source surface at $2.5 R_\odot$ to their counterparts at the photosphere, and that were obtained by potential field computations (Hakamada and Kojima, 1999). The field lines are indicated in red to show the footpoints of converging field lines during the traceback period corresponding to the central meridian passage dates at 1 AU when the solar wind was found to be highly non-radial. The curved black line represents the pseudostreamer locations estimated at the so-called source surface at $2.5 R_\odot$.

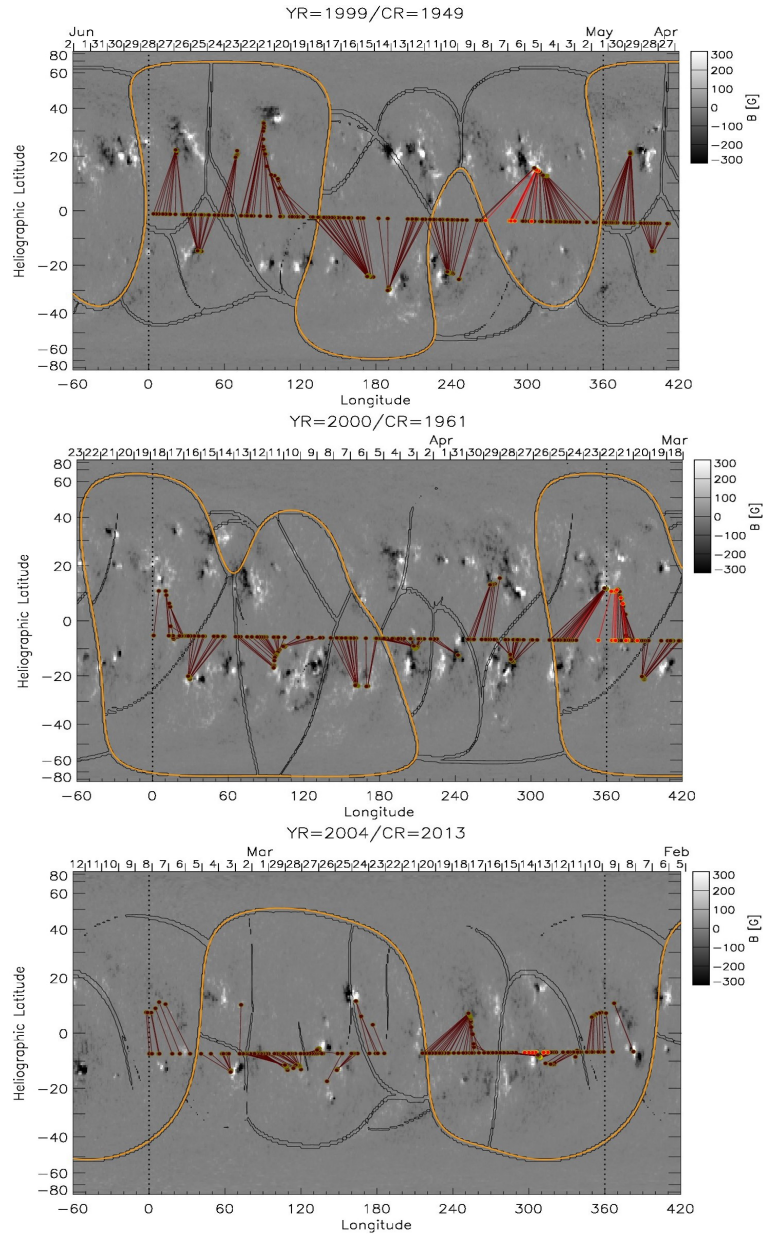It is evident from Fig. 3 that the back-projected photospheric footpoints, indicated by the

Figure 3: Synoptic maps, generated using SOHO/MDI magnetograms, during Carrington rotations CR 1949 (*top*), CR 1961 (*middle*), and CR 2013 (*bottom*) corresponding to the May 1999, March 2000, and February 2004 events. Regions of strong magnetic fields, corresponding to active region locations are depicted as black and white patches representing negative and positive magnetic polarities, respectively. The solid curved lines in yellow on each map are the source surface magnetic neutral lines. The groups of converging red and magenta lines depict magnetic field lines that join the source surface at $2.5\,R_\odot$ to their counterparts at the photosphere, and that were obtained by potential field computations (Hakamada and Kojima, 1999). The lines in red in each panel particularly indicate the footpoints of the converging field lines during the traceback period when the solar wind flow was highly non-radial.
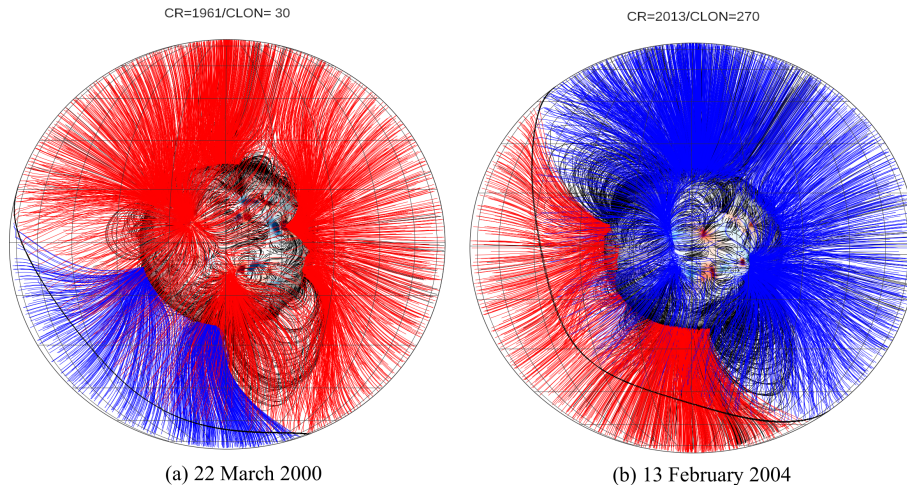
(a) 22 March 2000   (b) 13 February 2004

Figure 4: The 3D structure of coronal magnetic fields during the traceback dates for (a) 22 March 2000 in CR 1960 and (b) 13 February 2004 in CR 2013, viewed, respectively, from a central meridian passage longitude of $30°$ and $270°$.

converging field lines in red, during the traceback dates (5 May 1999, 21–22 March 2000, and 13 February 2004) for all the events originated in or around large active regions. Next, daily active region maps of the solar photosphere on the event and traceback dates were examined (not shown here). On the traceback date of 5 May 1999 corresponding to the event date of 11 May 1999, a large active region (AR 8525) was almost precisely located at the central meridian. Similarly, on the traceback dates of 23 March 2000 and 13 February 2004, large active regions (AR 8916 and AR 10554) were found to be located approximately $5°$ east of the central meridian. It is already known that the solar wind flows originating at the Sun's central meridian are usually Earth-directed (Janardhan et al., 2005). It is to be noted that the source ARs for all the events were located at or close to the central meridian (within $\sim 5°$–$10°$) when the solar wind flows became non-radial. It is argued that Earth-directed flows from an AR located east of the central meridian would take more time to transit across the central meridian (Janardhan et al., 2008a). Therefore, for the events of March 2000 and February 2004, the duration of non-radial flow is longer than in May 1999, where the corresponding AR was located at the central meridian.

The 3D coronal magnetic field configurations associated with the AR during the traceback dates of 22 March 2000 in CR 1960 and 13 February 2004 in CR 2013, viewed, respectively, from a CMP longitude of $30°$ and $270°$, are shown in Fig. 4. These magnetic field lines were obtained using a potential field source surface (PFSS) model (Hakamada and Kojima, 1999) and projected to a source surface at $2.5\,R_\odot$. In Fig. 4, the field lines in red and blue represent opposite polarities, with red indicating outward-going or positive fields and blue indicating inward-going or negative fields. The thin black lines represent closed magnetic field loops, while the thick black curve represents the source surface magnetic neutral line. Only field lines with magnitudes of 5–250 G are displayed. Similarly, the 3D coronal magnetic field structure on the traceback date of 5 May 1999 for the May 1999 non-radial event can be referenced

in Janardhan et al. (2005). The 3D coronal magnetic field configurations associated with the source AR of the respective events on the traceback dates clearly show open magnetic fields. The outward-going open field lines in red for the March 2000 event (see Fig. 4, left) and inward-going open field lines in blue for the February 2004 event (see Fig. 4, right) are observed to be associated with the AR. To better depict the uncluttered open field lines associated with the source AR of the non-radial flow events, the AR locations of the respective events shown in Fig. 4 are not precisely located at or close to the central meridian.

2.3. Source region evolutions

It is evident from Figs. 3 and 4 that the observed non-radial flow events at 1 AU are associated with large photospheric active regions and open field regions in the corona on the traceback periods. Additionally, it is observed from Fig. 2 that the non-radial flow source regions exhibit a transition from CH to AR. To investigate how the source regions of the non-radial flow events showed a transition from CH to AR, images from the the Extreme ultra-violet Imaging Telescope (EIT; Delaboudinière et al., 1995) at different wavelengths and MDI maps on board the SOHO spacecraft are plotted. In Fig. 5, the panels on the left and right, starting the top to bottom, show cut-off images of EIT 171 Å, EIT 195 Å, EIT 284 Å, and SOHO/MDI, respectively, for the event of May 1999. The images on the left correspond to the traceback date of 5 May 1999, while those on the right were taken 24-hours later (i.e., on 6 May 1999).

Similar figures were prepared for the March 2000 and February 2004 events (not shown here). The cut-off images of EIT for all the events show AR–CH complexes located at the central meridian. The corresponding photospheric changes of the evolving CH region for the 1999 May event are depicted in the bottom panel of Fig. 5. The magnetic field strength of the region displayed in the magnetogram has been limited to $\pm 300\,\mathrm{G}$. The image in the left panel was captured at 06:24:03 UT on 5 May 1999, while the image in the right panel was captured a little over 24 hours later, at 07:59:02 UT on 6 May 1999. Each panel's black and white regions correspond to negative and positive polarities. Corresponding to the location of the AR complex, as seen in the corona from the EIT image, is a small, white, circular region of strong magnetic fields located at the central meridian, which is part of a large bipolar magnetic region. On 6 May 1999, a new negative polarity, indicated by a black arrow, appeared north-west of the circular sunspot region. Correspondingly, the two bipolar regions located to the far west also appeared to evolve with new magnetic flux elements emerging. Similar to the May 1999 event, the corresponding photospheric changes of the evolving CH region for the March 2000 and February 2004 events (not shown) are observed. It is found that the March 2000 and February 2004 events also saw the emergence of new magnetic flux elements around the source region of interest.

Next, base difference images of the Sun from the EIT are obtained, as shown in Fig. 6 during the traceback periods of 5–8 May 1999, 21–23 March 2000 and 13–15 February 2004. These difference images were prepared by subtracting an image on the traceback date (called a reference image) from an image ~ 9 hours ahead of the reference image. There is no specific reason for using a 9-hour difference between the reference and base images. The evolutions in
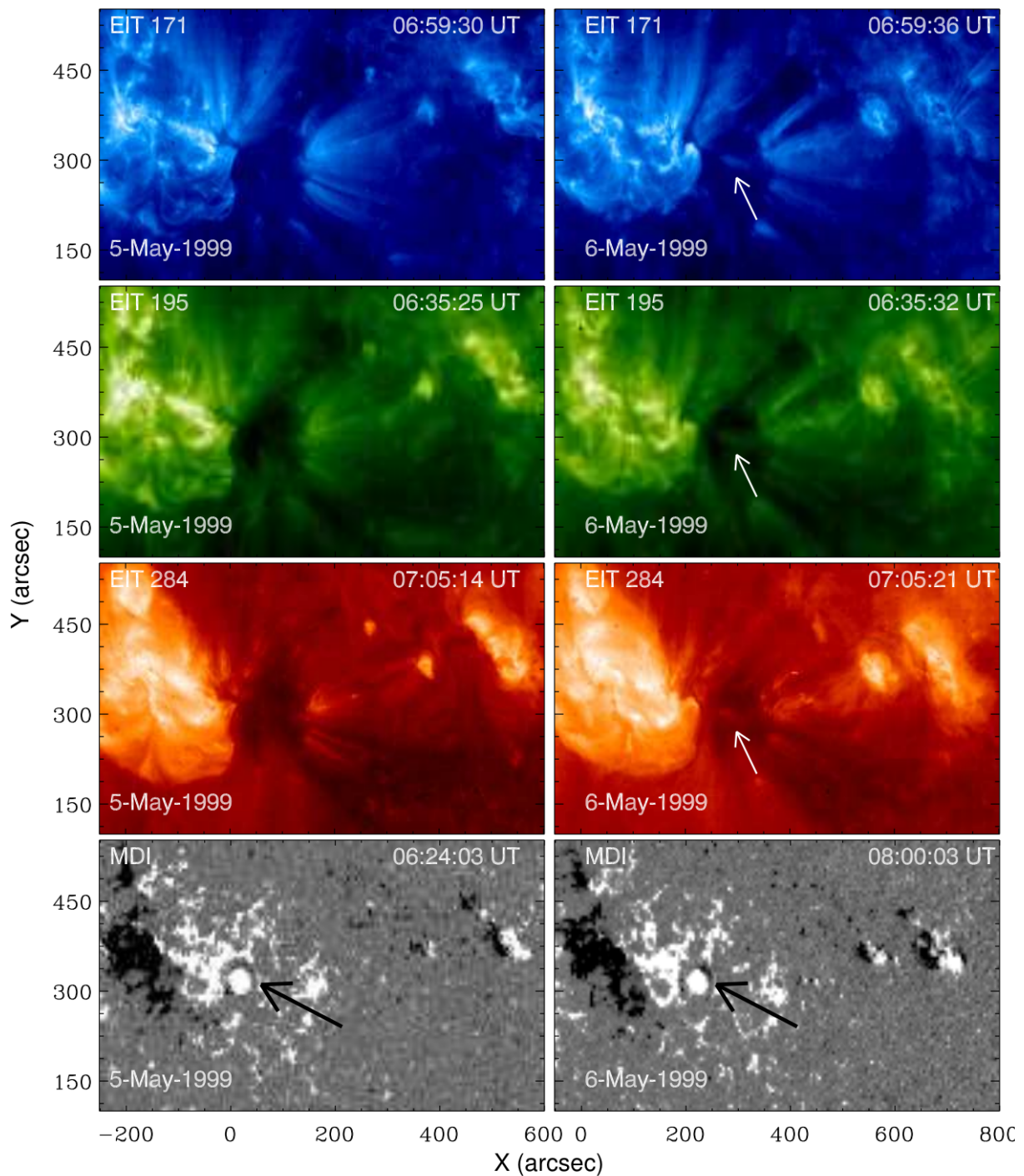
Figure 5: An image cut-out of the AR–CH complex region associated with the 11 May 1999 event. The images on the left and the right are, respectively, on the traceback date of 5 May 1999 and on the next day, 6 May 1999. The left and right panels, from top to bottom, show the images of EIT 171 Å, EIT 195 Å, EIT 284 Å, and SOHO/MDI, respectively. The white arrows in the top panels indicate the new CH features, while the black arrows mark the emergence of new magnetic fluxes.
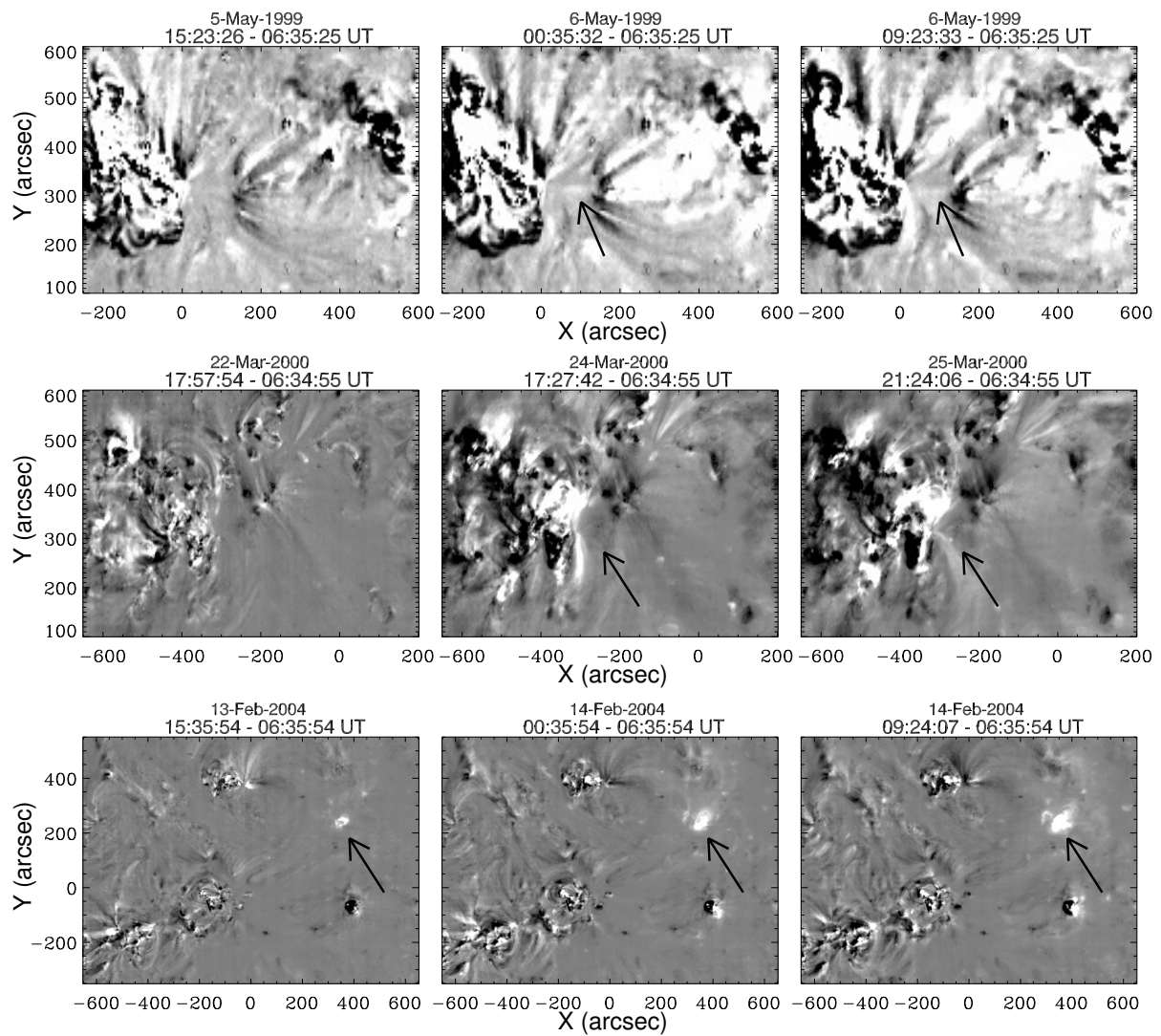
Figure 6: Base difference images obtained at an interval of 9 hours from EIT images corresponding to May 1999, March 2000, and February 2004 events. The arrows in the middle and right side panels mark changes in the CH region.

the AR–CH complexes were then investigated using the base difference images thus produced. The base difference images, prepared at a 9-hour difference, clearly show the evolutions of the features in the AR–CH complexes. Therefore, the 9-hour difference images are displayed in Fig. 6. The black regions in the base difference image are treated as regions of the reference image, while the white regions are considered new features. From Fig. 6, it is observed that CH regions were located close to or at the central meridian on the traceback dates. The very next day, new bright features emerged at the center of the CH region, as indicated by black arrows in the right-hand panels of Fig. 6. The new features observed in the base difference images 9 hours ahead of the reference image are perceived as constrictions or narrowing of the CH. Generally, CHs are regions of fast wind streams. With the emergence of the bright features in the CH, the area of the CH is further reduced. There is a high degree of correlation between solar wind speed and the size of the CH from which it emanates (Kojima et al., 1999) As a result, the flow speed of the stream originating from the CH is decreased further, and thus, the appearance of the bright features in the CH results in the emergence of the slow wind streams from the CH.

3. Discussion and Conclusion

The present study reports three extremely non-radial solar wind outflow events on 10–12 May 1999, 27–30 March 2004, and 15–18 February 2004. In all events, the average solar wind flow deviations from the radial direction exceeded $6°$ for a prolonged period between 24 and 48 hours, or longer. Prolonged and extremely non-radial flows were generally observed during CMEs and CIRs. However, none of these events were associated with CMEs and CIRs. In addition to the extremely non-radial flow, for all of the events, the solar wind flow velocities and densities were lower than usual during the duration of the non-radial flow. Such low-density and low-velocity solar wind flow phenomena have been studied earlier in the context of solar wind disappearance events (Balasubramanian et al., 2003; Janardhan et al., 2005, 2008a,b).

The oxygen charge-state ratio at L1 for all of the events increased from 0.2 to more than 0.2 just when the angle of radial solar wind flow exceeded $6°$, i.e., when the flow became highly non-radial. This observation suggests that the source regions must originate from AR–CH complexes so that the source of the solar wind flow can make a smooth transition from CH to AR (Schrijver and De Rosa, 2003; Janardhan et al., 2008a). Furthermore, the solar wind flows have been tracked from 1 AU to the source surface at $2.5 R_\odot$ using a constant velocity traceback method. Next, potential field computations applied to a synoptic magnetogram were used to trace back the footpoints of the magnetic field lines from the source surface to the photosphere. It is found that all of the events on the traceback dates of the events were associated with large ARs. Daily maps of the magnetogram on the corresponding traceback dates show that these source ARs were located at or close to the central meridian. Additionally, the three-dimensional magnetic field configurations of the Sun obtained using PFSS on the traceback dates indicate the presence of open field regions next to the ARs. On the other hand, the EIT cut-off images as well as the EIT base difference images on the traceback dates of the events have shown small, mid-latitude CHs adjacent to the large ARs. Furthermore, it is revealed from EIT images that the CHs evolved in time and showed the emergence of bright coronal loops. Similarly,

the MDI cut-off images on the traceback dates of the events show the emergence of opposite polarity magnetic flux elements on the photosphere close to the source ARs. The emergence of bright coronal loops progressively reduced the CH area. It is found that there was a high degree of correlation between solar wind speed and the size of the CH from which it emanated (Kojima et al., 1999). The reduction in the size of the CH would, therefore, suppress the CH outflow, giving rise eventually to a low-velocity solar wind stream. The rapid evolution observed in the CH complex before the start of the non-radial flow has been attributed to interchange reconnections. The reconnection occurs between the open unipolar CH fields and the closed bipolar magnetic flux regions (Janardhan et al., 2008b).

Based on our observations, we propose a possible explanation for the cause of the prolonged and highly non-radial flows. Generally, in a typical CIR, a compression region forms at the leading edge of the faster solar wind stream emanating from a CH when it overtakes the slower solar wind stream adjacent to it. However, in our case, due to the reduction in the size of the CH, the faster solar wind stream became even slower than the average slow solar wind flowing adjacent to it. Consequently, a compression region formed at the trailing edge of the significantly slower stream. As suggested by Pizzo (1989, 1991), the stream interface of CIRs acts like a slowly moving wall in the interplanetary medium. The compression region formed in our scenario acts as a slowly moving wall. Over time, as the source CH further reduces in size and eventually vanishes, leaving behind only the AR, this slowly moving wall is "pinched off" into the interplanetary space. The local interplanetary magnetic field, thus, is then diverted by this slowly moving wall (Lockwood et al., 2019) because of the prevailing low beta plasma condition with the magnetic field strength during the events being close to average and the very low solar wind density. As a result, the incoming solar wind flows follow the deflected magnetic field, possibly leading to extremely non-radial solar wind flow. Therefore, studying such prolonged and extremely non-radial solar wind events is crucial for gaining further insights into highly non-radial flows not associated with CMEs/CIRs.

Acknowledgments

Further Information

Authors' ORCID identifiers

0000-0002-9448-1794 (Susanta Kumar BISOI)
0000-0002-7820-7971 (Diptiranjan ROUT)

0000-0003-2504-2576 (Janardhan Padmanabhan)
0000-0002-7060-3750 (Ken'ichi Fujiki)
0000-0003-2693-5325 (Dibyendu Chakrabarty)

Author contributions

DR, PJ, and DC designed the project. DR, SKB, and PJ wrote and edited the manuscript. DR, KF, SKB, and KS performed the analyses and prepared the figures. DR, SKB, PJ, KF, and DC discussed the results and implications of the work at all stages.

Conflicts of interest

The authors declare no conflict of interest.

References

Balasubramanian, V., Janardhan, P., Srinivasan, S. and Ananthakrishnan, S. (2003) Interplanetary scintillation observations of the solar wind disappearance event of May 1999. JGRA, 108(A3), 1121. https://doi.org/10.1029/2002JA009516.

Delaboudinière, J.-P., Artzner, G. E., Brunaud, J., Gabriel, A. H., Hochedez, J. F., Millier, F., Song, X. Y., Au, B., Dere, K. P., Howard, R. A., Kreplin, R., Michels, D. J., Moses, J. D., Defise, J. M., Jamar, C., Rochus, P., Chauvineau, J. P., Marioge, J. P., Catura, R. C., Lemen, J. R., Shing, L., Stern, R. A., Gurman, J. B., Neupert, W. M., Maucherat, A., Clette, F., Cugnon, P. and van Dessel, E. L. (1995) EIT: Extreme-ultraviolet Imaging Telescope for the SOHO mission. SoPh, 162, 291–312. https://doi.org/10.1007/BF00733432.

Domingo, V., Fleck, B. and Poland, A. I. (1995) The SOHO mission: an overview. SoPh, 162, 1–37. https://doi.org/10.1007/BF00733425.

Gosling, J. T. and Pizzo, V. J. (1999) Formation and evolution of corotating interaction regions and their three dimensional structure. SSRv, 89, 21–52. https://doi.org/10.1023/A:1005291711900.

Hakamada, K. and Kojima, M. (1999) Solar wind speed and expansion rate of the coronal magnetic field during Carrington Rotation 1909. SoPh, 187, 115–122. https://doi.org/10.1023/A:1005183914772.

Janardhan, P., Fujiki, K., Kojima, M., Tokumaru, M. and Hakamada, K. (2005) Resolving the enigmatic solar wind disappearance event of 11 May 1999. JGRA, 110(A8), A08101. https://doi.org/10.1029/2004JA010535.

Janardhan, P., Fujiki, K., Sawant, H. S., Kojima, M., Hakamada, K. and Krishnan, R. (2008a) Source regions of solar wind disappearance events. JGRA, 113(A3), A03102. https://doi.org/10.1029/2007JA012608.

Janardhan, P., Tripathi, D. and Mason, H. E. (2008b) The solar wind disappearance event of 11 May 1999: source region evolution. A&A, 488(1), L1–L4. https://doi.org/10.1051/0004-6361:200809667.

Jian, L., Russell, C. T., Luhmann, J. G. and Skoug, R. M. (2006) Properties of stream interactions at one AU during 1995–2004. SoPh, 239(1-2), 337–392. https://doi.org/10.1007/s11207-006-0132-3.

Kahler, S. W. and Hudson, H. S. (2001) Origin and development of transient coronal holes. JGR, 106(A12), 29239–29248. https://doi.org/10.1029/2001JA000127.

Kojima, M., Fujiki, K., Ohmi, T., Tokumaru, M., Yokobe, A. and Hakamada, K. (1999) Low-speed solar wind from the vicinity of solar active regions. JGR, 104(A8), 16993–17004. https://doi.org/10.1029/1999JA900177.

Liewer, P. C., Neugebauer, M. and Zurbuchen, T. (2004) Characteristics of active-region sources of solar wind near solar maximum. SoPh, 223, 209–229. https://doi.org/10.1007/s11207-004-1105-z.

Lockwood, M., Owens, M. J. and Macneil, A. (2019) On the origin of ortho-gardenhose heliospheric flux. SoPh, 294(6), 85. https://doi.org/10.1007/s11207-019-1478-7.

Owens, M. and Cargill, P. (2004) Non-radial solar wind flows induced by the motion of interplanetary coronal mass ejections. AnGeo, 22, 4397–4406. https://doi.org/10.5194/angeo-22-4397-2004.

Pizzo, V. J. (1989) The evolution of corotating stream fronts near the ecliptic plane in the inner solar system. 1. Two-dimensional fronts. JGR, 94(A7), 8673–8684. https://doi.org/10.1029/JA094iA07p08673.

Pizzo, V. J. (1991) The evolution of corotating stream fronts near the ecliptic plane in the inner solar system. 2. Three-dimensional tilted-dipole fronts. JGR, 96(A4), 5405–5420. https://doi.org/10.1029/91JA00155.

Richardson, I. G. (2018) Solar wind stream interaction regions throughout the heliosphere. LRSP, 15, 1. https://doi.org/10.1007/s41116-017-0011-z.

Scherrer, P. H., Bogart, R. S., Bush, R. I., Hoeksema, J. T., Kosovichev, A. G., Schou, J., Rosenberg, W., Springer, L., Tarbell, T. D., Title, A., Wolfson, C. J., Zayer, I. and MDI Engineering Team (1995) The Solar Oscillations Investigation – Michelson Doppler Imager. SoPh, 162, 129–188. https://doi.org/10.1007/BF00733429.

Schrijver, C. J. and De Rosa, M. L. (2003) Photospheric and heliospheric magnetic fields. SoPh, 212(1), 165–200. https://doi.org/10.1023/A:1022908504100.